JM PAPERS

Identifying vortical network connectors for turbulent flow modification

Muralikrishnan Gopalakrishnan Meena[1,†] **and Kunihiko Taira**[1]

[1]Department of Mechanical and Aerospace Engineering, University of California, Los Angeles, CA 90095, USA

We introduce a network (graph) theoretic community-based framework to extract vortical structures that serve the role of connectors for the vortical interactions in two- and three-dimensional isotropic turbulence. The present framework represents the vortical interactions on a network, where the vortical elements are viewed as the nodes and the vortical interactions are regarded as edges weighted by induced velocity. We identify closely interacting vortical elements as vortical network communities through community detection algorithms. The inter- and intra-community interactions are used to identify the communities which have the strongest and weakest interactions amongst them. These vortical communities are referred to as the connector and peripheral communities, respectively. We demonstrate the influence of the network-based structures to modify the dynamics of a collection of discrete point vortices. Taking advantage of the strong inter-community interactions, connector community can significantly modify the collective dynamics of vortices through the application of multiple impulse perturbations. We then apply the community-based framework to extract influential structures in isotropic turbulence. The connector and peripheral communities extracted from turbulent flows resemble shear-layer and vortex-core-like structures, respectively. The influence of the connector structures on the flow field and their neighbouring vortical structures is analysed by adding impulse perturbations to the connectors in direct numerical simulations. The findings are compared with the cases of perturbing the strongest vortex tube and shear-layer regions. We reveal that perturbing the connector structures enhances local turbulent mixing beyond what is achieved by the other cases.

Key words: vortex interactions, isotropic turbulence, turbulence control

† Present address: National Center for Computational Sciences, Oak Ridge National Laboratory. Email address for correspondence: gopalakrishm@ornl.gov

1. Introduction

Analysis of turbulence remains as one of the most complex problems in science and engineering due to the strong nonlinear dynamics and multiscale properties of fluid flows (Hussain 1986). As turbulence is ubiquitous in nature and engineering problems, the modification of its dynamics has been an active field of study (Brunton & Noack 2015). For modelling and controlling their dynamics, it is important to understand the interactions amongst the vortical structures. Insights from such endeavors can support applications including flow separation control (Bhattacharjee, Scheelke & Troutt 1986) and mixing enhancement (Spencer & Wiley 1951). What makes this control problem challenging is that a large amount of energy is generally required to modify large-scale vortical structures to achieve flow modification.

To achieve flow modification with low levels of energy input, it is critical to identify important vortical structures in the flow. Various techniques have been introduced to extract flow structures. Reduced representation of the flow field using approaches such as the proper orthogonal decomposition (POD; Lumley 1967) and dynamic mode decomposition (DMD; Schmid 2010) has shown these tools as having great ability to extract the dominant features of the flow (Taira *et al.* 2017, 2020). Measures such as Q-criterion (Hunt, Wray & Moin 1988), λ_2-criterion (Jeong & Hussain 1995), Γ-criterion (Graftieaux, Michard & Grosjean 2001) and finite-time Lyapunov exponent (Haller 2005, 2015) can be used to identify highly rotational and strained regions of the flow (Dubief & Delcayre 2000; Chakraborty, Balachandar & Adrian 2005). Recently, machine-learning inspired methods have also been used to extract the dominant vortical structures in turbulence (Jiménez 2018).

Even with the available strategies to identify coherent structures, the quantification and analysis of vortical interactions is a challenge as every element in the flow field interacts with others. If the given flow field is spatially discretized into n discrete cells, the number of interactions amongst the cells to be accounted for will be $n(n-1)$. This is particularly crucial in turbulence with high dimensions. Graph theory provides a concrete mathematical framework for representing interactions amongst elements of a system as a network (Bollobás 1998). Valuable insights and models for high-dimensional systems, such as the brain networks, have been gained through graph-theoretic formulations (Barabási 2016). Moreover, the vast range of tools in network science enables the characterization, modelling and control of interaction-based dynamics (Newman 2010).

In recent years, network formulations have been introduced to quantify and capture the interactions in fluid flows. The induced velocity amongst vortical elements (Nair & Taira 2015), Lagrangian motion of fluid elements (Ser-Giacomi *et al.* 2015; Hadjighasem *et al.* 2016), oscillator-based representation of the energy fluctuations (Nair, Brunton & Taira 2018), time series of fluid-flow properties (Scarsoglio, Cazzato & Ridolfi 2017), triadic interactions in turbulence (Gürcan 2017; Gürcan, Li & Morel 2020) and the effects of perturbations on time-varying vortical flows (Yeh, Gopalakrishnan Meena & Taira 2020) have been studied using a network-theoretic framework. The formulations have been extended to characterize various turbulent flows, including two-dimensional isotropic turbulence (Taira, Nair & Brunton 2016), turbulent premixed flames and combustors (Godavarthi *et al.* 2017; Singh *et al.* 2017; Krishnan *et al.* 2019b), wall turbulence (Iacobello, Scarsoglio & Ridolfi 2018b), mixing in turbulent channel flow (Iacobello *et al.* 2018a, 2019a,b) and isotropic magnetohydrodynamic turbulence (Gürcan 2018). There have also been recent advances in using complex network analysis for turbulent flow control. Krishnan *et al.* (2019a) have used spatial correlation networks to mitigate oscillatory instabilities in turbulent reactive flows by identifying appropriate locations

for passive control strategies through various network measures. Also, Yeh *et al.* (2020) have utilized time-evolving vortical networks to identify dynamically relevant pathways to modify turbulent flows by combining formulations of Katz centrality and resolvent analysis.

Network-based clustering techniques have also been utilized to extract closely connected nodes and dominant features in fluid flows. Image sequences have been used to reconstruct the flow field using the Frobenius–Perron operator and community detection is implemented to identify key structures in the phase space (Bollt 2001). Spectral clustering has been considered for vortex detection in a Lagrangian-based framework of fluid-flow networks (Hadjighasem *et al.* 2016; Schneide *et al.* 2018). A coherent structure colouring technique also builds on a Lagrangian framework to identify coherent structures in complex flows (Schlueter-Kuck & Dabiri 2017; Husic, Schlueter-Kuck & Dabiri 2019). Gabriel graphs have also been used to compare and classify vortical flows based on topological similarities (Krueger *et al.* 2019). More recently, community detection has been used to extract vortical structures from complex flows (Murayama *et al.* 2018) and form reduced-order models for laminar wake flows (Gopalakrishnan Meena, Nair & Taira 2018; Gopalakrishnan Meena 2020).

A key attribute missing in clustering approaches is to take advantage of the inter- and intra-cluster interactions to identify the important interactions and clusters in the flow. Moreover, modifying the system dynamics by taking advantage of the interactions amongst the clusters has not yet been explored. In the present study, we use the intra- and inter-cluster interactions extracted from a network-based framework for identifying important flow-modifying vortical structures. We use the community detection algorithm (Gopalakrishnan Meena *et al.* 2018; Gopalakrishnan Meena 2020) to extract closely connected vortical elements in two- and three-dimensional isotropic turbulence. The interactions amongst the communities are used to identify key turbulent flow-modifying structures. The goal of this network-based framework is not to alter the global turbulent flow, but to influence certain key vortical structures in the complex background of isotropic turbulence.

A procedure for extracting the community-based structure for turbulent flows is illustrated in figure 1. In what follows, we first introduce the network representation of vortical interactions in § 2. We introduce the network-based measure of node strength and community detection to identify influential nodes in §§ 2.1 and 2.2, respectively. The importance of the network-based measures is discussed within the context of a model problem of ideal point-vortex dynamics. We assess the influence of the identified nodes to modify the dynamics of a collection of discrete point vortices in § 3. We then employ the network community-based formulation to extract influential structures in two- and three-dimensional isotropic turbulence, described in § 4. The numerical set-ups are discussed in § 4.1. We characterize the vortical network of two- and three-dimensional isotropic turbulence in § 4.2. We then demonstrate the use of community-based structures to modify the turbulent flows in § 4.3. Finally, concluding remarks are provided in § 5.

2. Network-theoretic description of vortical interactions

To identify the influential regions to perturb for flow modification, we examine the interactions amongst the vortical elements. We discretize the vorticity field in a Lagrangian and Eulerian perspective. The discrete vortical elements are referred to as nodes in the present work. To quantify the interactions amongst the vortical nodes, we consider the induced velocity imposed upon each other. The Biot–Savart law provides the induced velocity from a vortical element as a function of circulation and relative position of the
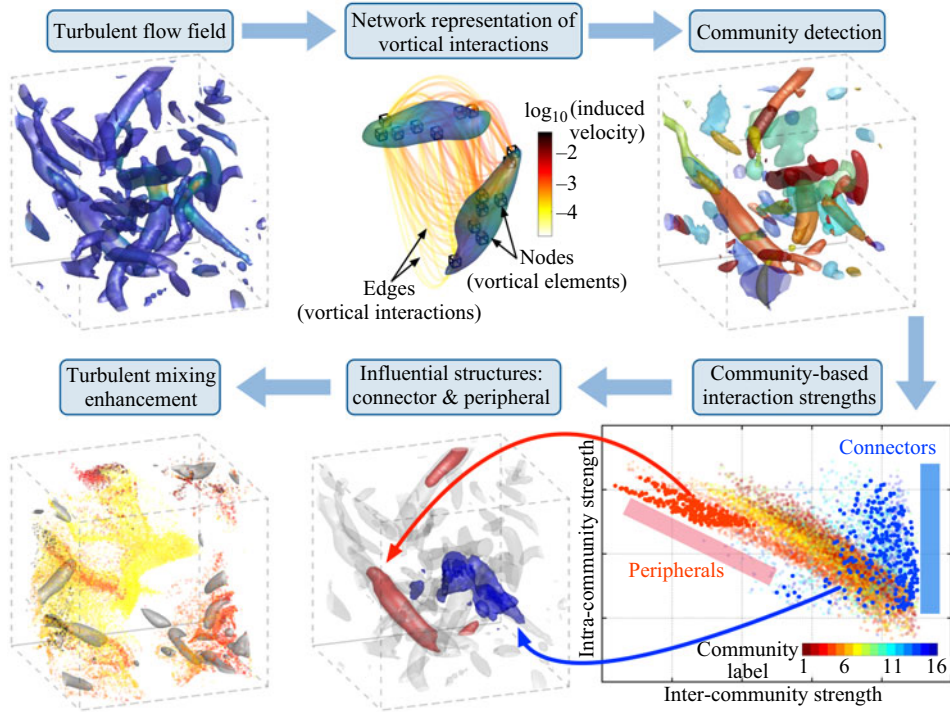
Figure 1. An overview of the community-based procedure for extracting turbulent-flow-modifying structures.

vortical elements, expressed as

$$u(r, t) = \frac{1}{2(n_d - 1)\pi} \int_V \frac{\omega(r', t) \times (r - r')}{\|r - r'\|_2^{n_d}} \, dV',\qquad(2.1)$$

where $u(r, t)$ is the induced velocity at location r in the domain from a collection of vortical elements enclosed in volume V with a vorticity distribution of $\omega(r', t)$ at positions r'. Here, n_d is the spatial dimension of the flow field and $\|\cdot\|_2$ denotes the Euclidean norm. Furthermore, the influence of a vortical node (element) i on node j is evaluated as

$$u_{j \leftarrow i} = \frac{1}{2(n_d - 1)\pi} \int_{V_i} \frac{\omega(r', t) \times (r_j - r')}{\|r_j - r'\|_2^{n_d}} \, dV',\qquad(2.2)$$

where $u_{j \leftarrow i}$ denotes the velocity induced from vortical node i to j and V_i represents the volume of vortical node i. As an example, we illustrate the interactions between two vortical nodes in figure 2. The vortical structures are visualized by the isosurface of Q-criterion, $Q = \frac{1}{2}[\|(\nabla u - \nabla u^T)\|_2^2 - \|(\nabla u + \nabla u^T)\|_2^2]$ (Hunt *et al.* 1988), and coloured with the magnitude of vorticity $\|\omega\|_2$. Here, element i has higher vorticity magnitude compared with element j. Thus, the magnitude of velocity induced by i onto j is higher than that imposed by j onto i, yielding an asymmetric interaction.

Characterizing the interaction-based behaviour of vortical elements can be a challenge in high-Reynolds-number turbulence, particularly with high degrees of freedom needed to discretize the flows. To facilitate the analysis of high-dimensional dynamics, we leverage the analytical approaches in graph theory (Bollobás 1998) and network science (Newman 2010). Here, we establish a network-theoretic representation of the vortical interactions in
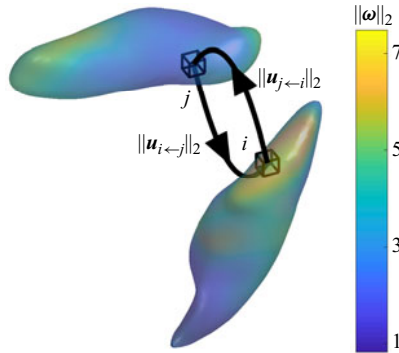
Figure 2. Interactions between two vortical elements in vortical structures extracted from three-dimensional isotropic turbulent flow. The vortical structures are visualized by isosurface of Q-criterion coloured with the magnitude of vorticity $\|\boldsymbol{\omega}\|_2$. The vortical elements are shown for the spatial grid cells.

a flow field. We construct a network (graph) $\mathscr{G}$ comprising vortical nodes $\mathscr{V}$ connected by edges $\mathscr{E}$ holding edge weights $\mathscr{W}$ based on induced velocity. Given this definition $\mathscr{G} = \mathscr{G}(\mathscr{V}, \mathscr{E}, \mathscr{W})$ for the network, we can quantify the important nodes in vortical flows.

The collection of connectivity amongst the nodes can be represented by the adjacency matrix $\boldsymbol{A}$, which holds the edge weights as its elements. For the vortical interaction network, $\boldsymbol{A}$ is defined using the normalized magnitude of induced velocity (Nair & Taira 2015; Taira *et al.* 2016) as

$$A_{ij} = \frac{\|\boldsymbol{u}_{i \leftarrow j}\|_2}{u^*}, \tag{2.3}$$

where u^* is a characteristic velocity of the flow. For a flow field with n vortical nodes, the adjacency matrix $\boldsymbol{A} \in \mathbb{R}^{n \times n}$. The above formulation gives an asymmetric adjacency matrix, representing a directed network. Adding directions to the links helps differentiate between the influential and influenced nodes. Non-dimensionalization is important for the analysis of turbulent flows over a range of Reynolds number. The details of the non-dimensionalization will be discussed in § 4.

Let us discuss the role of $\boldsymbol{A}$ on network dynamics and appropriate measures to identify influential nodes. Consider a general dynamical system for n state vectors $\boldsymbol{x}_i \in \mathbb{R}^{p_v}$ holding p_v variables over a network. The general interaction-based dynamics of the elements can be expressed as

$$\dot{\boldsymbol{x}}_i = \boldsymbol{f}(\boldsymbol{x}_i) + \sum_{j=1}^{n} A_{ij} \boldsymbol{g}(\boldsymbol{x}_i, \boldsymbol{x}_j), \quad i = 1, 2, \ldots, n, \tag{2.4}$$

where function $\boldsymbol{f}(\boldsymbol{x}_i)$ represents the intrinsic dynamics of node i and function $\boldsymbol{g}(\boldsymbol{x}_i, \boldsymbol{x}_j)$ describes the interactive dynamics between nodes i and j. We consider the model fluid-flow problem of ideal point-vortex dynamics (Aref 2007; Newton 2013) to demonstrate the interaction-based dynamics of vortical elements and identify important vortical nodes using the network-based approach.

Let us take a collection of $n = 100$ discrete point vortices, initialized on an infinite two-dimensional domain as shown in figure 3(*a*). These vortices are initially arranged into five groups initial time instant. The vortices are coloured by their circulations $\Gamma_i = \omega_i \Delta S$, which is kept constant over time in the inviscid flow. Here, the vortical elements have the same area ΔS. The circulations have a normal distribution about a mean of $\overline{\Gamma} = 0.1$ and a standard deviation of $\sigma_\Gamma = 0.008$. This canonical model problem portrays the
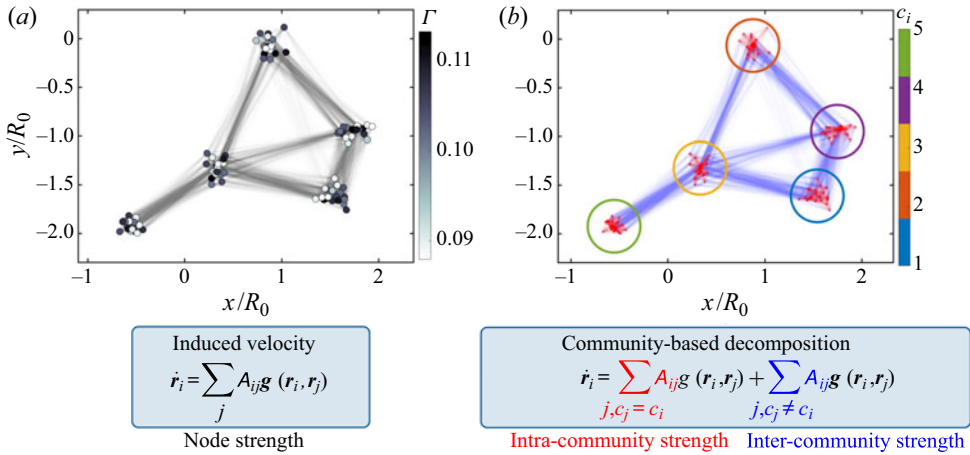
Figure 3. Interactions amongst a collection of discrete point vortices are used to illustrate the decomposition of networked dynamics through intra- and inter-community interactions.

nonlinear dynamics of vortical structures found in various flows (Nair & Taira 2015). The transparent grey edges visualize all interactions amongst the nodes, based on (2.3). Here, we use $u^* = |\Gamma_{tot}|/(2\pi R_0)$ where $\Gamma_{tot} = \sum_i^n \Gamma_i$ is the total circulation of the system and R_0 is the average radial distance of the centroid of the clusters from the geometric centre of the overall system at initial condition. The spatial variables are non-dimensionalized by R_0. The Biot–Savart law governs the dynamics of the point vortices, which can be expressed in terms of (2.4) for which $f(r_i) = 0$, $A_{ij} = |\Gamma_j|/(2\pi u^* \|r_i - r_j\|_2)$ and $g(r_i, r_j) = u^* \hat{k} \times (r_i - r_j)/\|r_i - r_j\|_2$. Here, $\hat{k}$ is the out-of-plane unit normal vector. We use this dynamical systems example to demonstrate the evaluation of important network measures pertinent to the interactive dynamics of the vortical elements.

2.1. Node strength

The node strength measures the ability of a node to be influential (out-strength) or be influenced (in-strength) in the network. The out- and in-strengths of a node are defined by

$$s_i^{out} = \sum_j A_{ji} \quad \text{and} \quad s_i^{in} = \sum_j A_{ij}, \tag{2.5a,b}$$

respectively. These measures are useful to identify the node with a collection of significant connections in a network.

For the vortical networks, the present definition of edge weight from (2.3) is based on the out-weight, which is used to evaluate the out-strength. Herein, the node strength, s_i, is taken to be the out-strength, unless specified otherwise. A relation between the node strength and enstrophy, $\Omega(r, t) = \|\omega(r, t)\|_2^2$, of a vortical element can be obtained using (2.2) as

$$s_i = \frac{1}{2(n_d - 1)\pi u^*} \sum_j \left\| \int_{V_i} \frac{\omega(r', t) \times (r_j - r')}{\|r_j - r'\|_2^{n_d}} \, dV' \right\|_2, \tag{2.6a}$$

$$\cong \frac{1}{2(n_d - 1)\pi u^*} \sum_j \left\| \int_{S_i} \|\omega(r', t)\|_2 \hat{e}_{\omega(r',t)} \, dS' \times \frac{(r_j - r_i)}{\|r_j - r_i\|_2^{n_d}} \Delta l_i \right\|_2, \tag{2.6b}$$

$$= \frac{|\Gamma_i| \Delta l_i}{2(n_d - 1)\pi u^*} \sum_j \frac{\|\hat{\boldsymbol{e}}_{\boldsymbol{\omega}_i} \times \hat{\boldsymbol{e}}_{\boldsymbol{r}_j - \boldsymbol{r}_i}\|_2}{\|\boldsymbol{r}_j - \boldsymbol{r}_i\|_2^{(n_d - 1)}}, \tag{2.6c}$$

$$= \frac{\sqrt{\Omega_i} \Delta V_i}{2(n_d - 1)\pi u^*} C, \tag{2.6d}$$

where $\hat{\boldsymbol{e}}_{(\cdot)}$ denotes the unit vector in the direction of $(\cdot)$, Δl_i is the length of vortical element i, and the sum of distance components is denoted by $C = \sum_j \|\hat{\boldsymbol{e}}_{\boldsymbol{\omega}_i} \times \hat{\boldsymbol{e}}_{\boldsymbol{r}_j - \boldsymbol{r}_i}\|_2 / \|\boldsymbol{r}_j - \boldsymbol{r}_i\|_2^{(n_d - 1)}$, which is constant for a fully periodic domain. Here, we assume that the vortical element j is sufficiently distant from the vortical element i such that $(\boldsymbol{r}_j - \boldsymbol{r}') / \|\boldsymbol{r}_j - \boldsymbol{r}'\|_2^{n_d}$ is constant over the vorticity concentration of i, giving rise to (2.6b) (Kundu, Cohen & Dowling 2011). This relationship reveals that $s_i \propto \sqrt{\Omega_i}$. This is particularly useful to determine the node strength distribution $p(s)$ of a vortical network, computation of which becomes prohibitively expensive for networks comprising large number of edges, such as turbulent flows of high Reynolds number. The distribution is dependent on the enstrophy distribution $p(\Omega)$. The latter is usually a known or measurable flow statistics. Distribution $p(s)$ gives a global picture of the nature of connectivity in the network and is used to identify the type of the network (Barabási 2016). The distribution is also useful to identify the node with the highest interaction strength, $\max_i s_i$, which is referred to as the hub node of a network. These nodes have been found to be important in assessing the robustness of the network dynamics against random and targeted perturbations (Albert, Jeong & Barabási 2000; Taira *et al.* 2016).

2.2. *Community detection*

Identifying closely connected vortical nodes is important towards revealing key local groups on the network. Such modular groups of nodes with high connectivity amongst each other are referred to as communities (Newman & Girvan 2004). One approach to find the communities is to measure the overall modular nature of a network using modularity M (Leicht & Newman 2008) given by

$$M = \frac{1}{2n_e} \sum_{ij} \left[A_{ij} - \gamma_M \frac{s_i^{in} s_j^{out}}{2n_e} \right] \delta(c_i, c_j), \tag{2.7}$$

where n_e is the total number of edges in the network, γ_M is the modularity resolution parameter to weigh the presence of small or large communities in the network (Reichardt & Bornholdt 2006; Fortunato & Barthélemy 2007), $\delta(c_i, c_j)$ is the Kronecker delta, $c_i \in \hat{C}_k$ is the label of the community to which element i is assigned and $\hat{C}_k$ is the set of k-th network community. Here, $k = 1, 2, \ldots, m$, with m being the total number of communities. The communities can be identified by maximizing M by regrouping the nodes. Here, the number of communities m is unspecified and determined by the algorithm. Various algorithms are available to identify the communities in a network (Fortunato 2010). In the present study, we adopt the method by Blondel *et al.* (2008) to identify the communities in large vortical networks with accuracy and low computational cost (Fortunato 2010). We herein refer to these network communities on vortical networks as the vortical communities (Gopalakrishnan Meena *et al.* 2018). Also, for vortical flows, γ_M can be set based on the plateau effect on the number of vortical communities identified with change in γ_M for a given Reynolds number.

The community information can then be used to decompose the term with the adjacency matrix in (2.4) as

$$\dot{x}_i = f(x_i) + \sum_{j,c_j=c_i} A_{ij}g(x_i, x_j) + \sum_{j,c_j \neq c_i} A_{ij}g(x_i, x_j). \tag{2.8}$$

The second term on the right-hand side represents the interaction of node i with the nodes in its own community, and the third term denotes the interaction of node i with the nodes in the other communities. The former represents the intra-community interactions and the latter term captures the inter-community interactions of node i. This gives a community-based dynamical systems equation for the elements of a network, emphasizing local influences of the communities. An illustration of the above procedure applied to the system of point vortices is shown in figure 3. The network with no distinction of the weighted edges is shown in figure 3(*a*). The community detection algorithm classifies the nodes into several communities, highlighted by the coloured circles in figure 3(*b*). The intra- and inter-community edges are shown in red and blue, respectively.

Let us quantify the local influence of a node using the above formulation. Similar to how the node strength is defined in (2.5*a,b*), the strength of node i to influence all nodes in community k can be defined as

$$s_{i,k} = \sum_{j,c_j \in \hat{C}_k} A_{ji}. \tag{2.9}$$

Moreover, the strength of a node on the network can be separated into intra- and inter-community strengths as

$$s_i^{intra} = \sum_{j,c_j=c_i} A_{ji} = s_{i,c_i} \quad \text{and} \quad s_i^{inter} = \sum_{j,c_j \neq c_i} A_{ji} = \sum_{k,k \neq c_i} s_{i,k}, \tag{2.10a,b}$$

respectively. These community-based strengths can be used to quantify the interactions with respect to communities.

The intra-community strength can be normalized as the within-module z-score (Guimera & Amaral 2005) given by

$$Z_i = \frac{s_i^{intra} - \overline{s_i^{intra}}}{\sigma_{s_i^{intra}}}, \tag{2.11}$$

where $\overline{s_i^{intra}}$ and $\sigma_{s_i^{intra}}$ are the mean and standard deviation of s_i^{intra} over all nodes in the community of i. The within-module z-score identifies the most well-connected node inside a community or the hub node of a community. Note that the hub node of a community need not be well-connected with the other communities in the network.

A relative measure of inter-community strength of a node, quantified by how well-distributed its edges are amongst communities, can be given by the participation coefficient (Guimera & Amaral 2005)

$$P_i = 1 - \left[\left(\frac{s_i^{intra}}{s_i} \right)^2 + \sum_{k,k \neq c_i} \left(\frac{s_{i,k}}{s_i} \right)^2 \right]. \tag{2.12}$$

When $P_i \approx 1$, edge weights of node i are equally connected among all communities, and $P_i = 0$ when the node is only connected to its own community. Note that $s_{i,k}$, Z_i and P_i
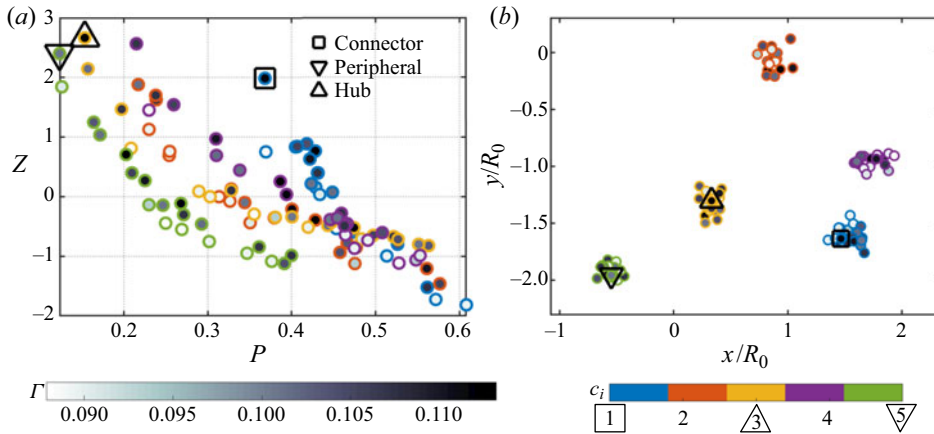
915 A10-8

Figure 4. (*a*) *P*–*Z* map for the discrete point vortices. The influential connector ($\square$), peripheral ($\triangledown$) and hub ($\triangle$) nodes are also identified. (*b*) Position of the important nodes in physical space.

can be evaluated for both in- and out-edges. In the present study, we evaluate the out-edge based measures following the definition of edge weight from (2.3).

The *P*–*Z* map of a network, comprising P_i and Z_i values of all the nodes on the network, is an important feature space for revealing key elements within and amongst the communities (Guimera *et al.* 2005; Fortunato 2010; Rubinov & Sporns 2010). The plot shows the P_i and Z_i values on the horizontal and vertical axes, respectively. This map identifies influential nodes based on their relative importance in influencing their own community and other communities in the network through intra- and inter-community interactions, respectively. For vortical networks, high intra-community influence of vortical elements can be understood as the ability to significantly affect the behaviour of their own vortical structure by imparting self-induced velocity on the other elements with the same structure. Whereas, high inter-community interaction of vortical elements can be interpreted as the ability to impart high induced velocity on other vortical structures.

The *P*–*Z* map for the system of point vortices is shown in figure 4(*a*). The nodes on the left side of the *P*–*Z* map have very low inter-community interactions and are isolated groups, called peripherals. On the other hand, the nodes on the right side have high inter-community interactions, making them well-connected to most communities and are called connectors. The nodes on the top region with high *Z* value have the strongest interactions within the respective communities. Note that the name peripheral need not refer to nodes at the physical perimeter of the domain. The strongest peripheral nodes will have high influence within their communities but the least influence on other communities. In contrast, the strongest connector nodes will have the highest influence amongst communities, particularly on the neighbouring communities (in spatial proximity), and high influence within their own community.

We use the *P*–*Z* feature space to search for the strongest peripheral and connector nodes in a network, herein referred to as simply peripheral and connector nodes. We find the average P_i of each community *k*, denoted as $\overline{P_k}$. The peripheral node of a network is the node *i* given by $\max_{i,c_i=k} Z_i$, belonging to the community *k* with $\min_k \overline{P_k}$. The connector node *i* is given by $\max_{i,c_i=k} Z_i$, belonging to community *k* with $\max_k \overline{P_k}$. The connector, peripheral, and hub nodes of the discrete point-vortex system are indicated in figure 4(*a*). The *P*–*Z* values for the nodes suggest that the hub node would have similar characteristics as the peripheral node. The three important nodes are also highlighted in the physical

space as shown in figure 4(*b*). The positions of the peripheral and connector nodes suggest that an influential node need not be located at the geometric centre of the community. The observations signify the need to consider inter- and intra-community interactions for identifying important nodes. Let us now demonstrate how the behaviour of the networked system can be modified using these measures.

3. Community-based modification of discrete point-vortex dynamics

We analyse the influence of the connector, peripheral and hub nodes identified using the network-based measures on the dynamics of a collection of discrete point vortices. We consider the same model problem set-up with $n = 100$ discrete point vortices used in § 2. Velocity-based impulse perturbations are added to all nodes of the identified influential community. Based on the community being perturbed, we refer to the forcing input as connector, peripheral or hub-based perturbation. Positions of the perturbed communities at the initial time instant are shown in figure 4(*b*). We identify the influential nodes only at the initial time instant as we are interested in exploring the influence of the nodes on the system dynamics.

Impulse perturbations at discrete time $n_t \Delta t$ are added to the velocity field with time step Δt and $n_t = 0, 1, 2, \ldots$. The velocity of a perturbed node i at time t is given by $\boldsymbol{u}(\boldsymbol{r}_i, t) + \tilde{\boldsymbol{u}}(\boldsymbol{r}_i, t)$, where $\tilde{\boldsymbol{u}}(\boldsymbol{r}_i, t) = \alpha \hat{e}_{\boldsymbol{u}(\boldsymbol{r}_i,t)} \delta(t - n_t \Delta t)$, α is the amplitude of perturbation, and $\hat{e}_{\boldsymbol{u}(\boldsymbol{r}_i,t)}$ is the unit vector in the direction of $\boldsymbol{u}(\boldsymbol{r}_i, t)$. Time is non-dimensionalized as $t \Gamma_{tot}/(2\pi R_0^2)$. Amplitude of perturbation α is computed for a given energy ratio E of

$$E = \frac{\displaystyle\sum_{i, c_i \in \hat{C}_p} \|\tilde{\boldsymbol{u}}(\boldsymbol{r}_i, t)\|_2^2}{\displaystyle\sum_i^n \|\boldsymbol{u}(\boldsymbol{r}_i, t)\|_2^2}, \tag{3.1}$$

where $\hat{C}_p$ is the set of the perturbed community. We have analysed the system dynamics with E varied between 0.01–0.1 and have found qualitative similarity in the results. Here, we show the results of perturbations with $E = 0.1$ to portray significant changes in the vortex trajectories. The time step between each perturbation is $\Delta t \Gamma_{tot}/(2\pi R_0^2) = 0.024$.

The effect of the perturbations on system dynamics is assessed by observing the change in trajectories of the community centroids, as shown in figure 5(*a*–*c*). The centroid location $\boldsymbol{\xi}_k(t)$ of each community k is computed as

$$\boldsymbol{\xi}_k(t) = \frac{\displaystyle\sum_{i, c_i \in \hat{C}_k} \Gamma_i \boldsymbol{r}_i(t)}{\displaystyle\sum_{i, c_i \in \hat{C}_k} \Gamma_i}. \tag{3.2}$$

The connector-based perturbations achieve the largest deviations on the trajectories as shown in figure 5(*a*). The peripheral and hub-based perturbations have significant influence only on their neighbouring communities, communities 3 and 1, respectively, as evident from figures 5(*b*) and 5(*c*). Regardless of the central location of the hub community at the initial time instant, the system dynamics is not changed compared with the extent achieved by connector-based perturbations. This demonstration highlights the need to consider the strengths and relative positions in a systematic manner to identify the influential nodes.
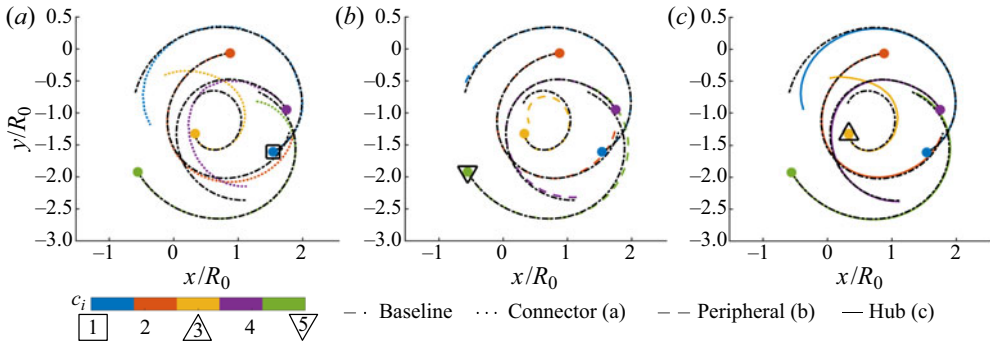
915 A10-10

Figure 5. Trajectories of community centroids with perturbations added to (*a*) connector ($\square$), (*b*) peripheral ($\triangledown$) and (*c*) hub ($\triangle$) communities. Filled circles show initial position of the community centroids.
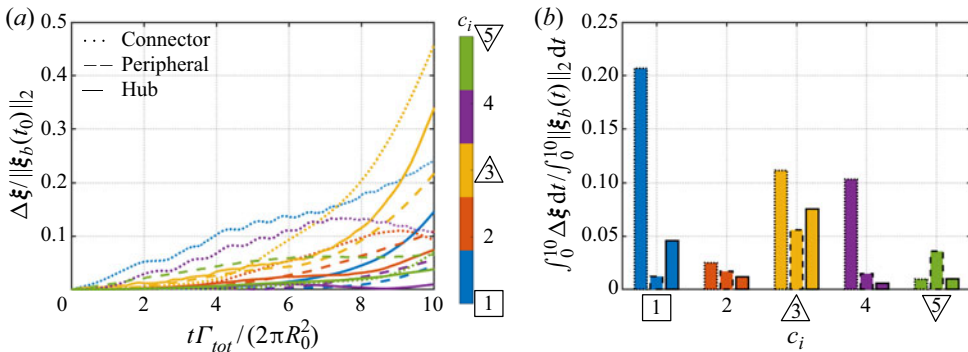

Figure 6. (*a*) Trajectories of community centroids subjected to connector ($\square$), peripheral ($\triangledown$) and hub-based ($\triangle$) perturbations compared with baseline, $\boldsymbol{\xi}_b$. Here, $\Delta\boldsymbol{\xi} = \|\boldsymbol{\xi}(t) - \boldsymbol{\xi}_b(t)\|_2$. (*b*) Total change in trajectory of community centroids with respect to the baseline.

Let us compare the community centroid trajectories in time, as shown in figure 6(*a*). The trajectories of all other communities show the most deviation from baseline with connector-based perturbation, except for community 5. The trajectory of community 5, the peripheral community, is modified significantly when it is perturbed. We have evaluated the *P–Z* map using the in-edges (not shown), which also gives community 5 to be the peripheral community. Thus, other communities have less influence on community 5. We concentrate on the results during early time instants to assess the characteristics of the connector to influence its neighbour and connect with other communities. The trajectory of community 4 is changed significantly at early time instants with connector-based perturbations. This change in trajectory of community 4, the spatially closest community to the connector, at early time instants demonstrates the ability of a connector community to significantly influence its neighbour. Neither of the peripheral and hub-based perturbations influence other communities, particularly their respective neighbours, at early times. Later, the connector-based perturbations also significantly change the dynamics of community 3 by connecting through community 4, even though communities 1 and 3 are spatially far apart. The inter-community influence demonstrates the connecting characteristics of a connector community.

Deviation of the trajectories from baseline is quantified in figure 6(*b*). The observations quantitatively show the larger deviations in trajectories resulting from connector-based perturbations. Considering the neighbours of the perturbed communities, a total

change between 10–12 % of the baseline is achieved for communities 3 and 4 using connector-based perturbations. The corresponding changes using peripheral and hub-based perturbations are around 5 % for communities 3 and 1, respectively. The largest effect of the hub community is on its own trajectory. These observations demonstrate the inference from the *P–Z* map that the hub community can portray characteristics of a peripheral. The magnitude of change achieved by the connector-based perturbation on its own trajectory is more than three times that produced by peripheral and hub communities. Furthermore, the total change in trajectory of community 3 is the highest using connector-based perturbation. For this model problem, we have demonstrated that the connector node effectively modifies the global vortex dynamics. The present finding motivates the use of inter-community interactions to instigate changes in the global system dynamics, based on the community-based decomposition of system dynamics to identify key structures.

4. Community-based flow modification of isotropic turbulence

Let us now consider the application of community-based flow modification to two- and three-dimensional decaying homogeneous isotropic turbulence. The highly complex and multiscale properties of isotropic turbulence make it an apt choice to demonstrate the capability of the present community-based framework. Isotropic turbulence is a canonical model problem for a range of turbulent flows encountered in nature and engineering applications.

4.1. *Numerical set-up*

For the two- and three-dimensional decaying isotropic turbulent flows, we use the Fourier spectral and pseudo-spectral algorithms, respectively, to numerically solve the Navier–Stokes equations (Chumakov 2008; Taira *et al.* 2016). Direct numerical simulations (DNS) of the unforced flows are performed in bi-periodic and tri-periodic square and cubic domains of length *L*. For the simulations, the flow fields are resolved such that $k_{max}\eta \geqslant 1$, where k_{max} is the maximum resolvable wavenumber of the grid and η is the Kolmogorov length scale. We non-dimensionalize the spatial variables by *L* and time by the large-eddy turn-over time at the initial time instant $\tau_e(t_0)$.

The two-dimensional DNS are initialized with a smooth distribution comprising approximately 100 superimposed Taylor vortices with random strengths, core sizes and locations. The flow field satisfies the kinetic energy spectra $E(k) \propto k \exp(-k^2/k_0^2)$, where $k_0 = 26.5$ (Kida 1985; Brachet, Meneguzzi & Sulem 1986). The three-dimensional DNS are initialized with random velocity fields of Gaussian p.d.f. profiles satisfying incompressibility and the Kolmogorov spectra for kinetic energy, $E(k) \propto k^{-5/3}$. The two- and three-dimensional simulations are run from these initial conditions until the flows are in the decaying regime, after which data are collected to perform the network analysis.

The two-dimensional turbulent flows with an initial Taylor microscale-based Reynolds number of $Re_\lambda(t_0) \approx 4000$ are obtained from DNS performed at a grid resolution of 1024×1024. We use snapshots of the vorticity field, uniformly subsampled to a resolution of 128×128, to construct the vortical network. For three-dimensional isotropic turbulence, flow fields with $Re_\lambda(t_0) \approx 40$ are obtained from DNS performed with a grid resolution of $64 \times 64 \times 64$. The three-dimensional flow fields are uniformly subsampled to a resolution of $32 \times 32 \times 32$ for constructing the vortical network.
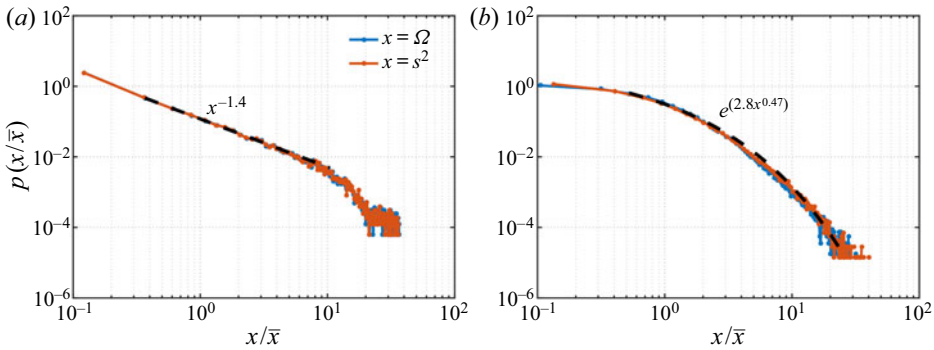
Figure 7. Probability distributions of enstrophy and node strength (squared), normalized by their mean values, of (*a*) two- and (*b*) three-dimensional isotropic turbulence.

Subsampling is performed in a manner such that the network representation is not influenced.

The network representation can be made independent of the Reynolds number following the non-dimensionalization of the edge weights using (2.3). We choose the characteristic velocity

$$u^* = V^{1/n_d} \Omega_{tot}^{1/2} = V^{1/n_d} \left(\frac{\int_{\|\boldsymbol{\omega}\|_2 \geqslant \omega_{th}} \|\boldsymbol{\omega}(\boldsymbol{r}, t)\|_2^2 \, \mathrm{d}V}{V} \right)^{1/2}, \tag{4.1}$$

where Ω_{tot} is the total enstrophy per unit area or volume of all the vortical elements enclosed in a region of vorticity threshold ω_{th}. We concentrate on vortical elements with high vorticity (McWilliams 1984), extracted through vorticity thresholding (Jiménez *et al.* 1993). We can capture the overall interaction behaviour of the flow field even with the threshold. For both two- and three-dimensional flow fields, we use a threshold of $\omega_{th} = 0.05 \|\boldsymbol{\omega}(\boldsymbol{r})\|_\infty$. Detailed assessment on the influence of the Reynolds number, grid and ω_{th} is provided in the Appendix.

4.2. *Network characterization of isotropic turbulence*

Let us first characterize the interactions amongst the vortical elements in two- and three-dimensional isotropic turbulence. Following (2.6), we evaluate the node strength and enstrophy distributions of the flow fields at an instant in time, presented in figure 7. The enstrophy and square of node strength are normalized by their respective mean values. The node strength-enstrophy relations from (2.6) are shown here for isotropic turbulence. Benzi, Patarnello & Santangelo (1987) found a power-law profile for the enstrophy distribution of two-dimensional decaying isotropic turbulence. The distribution $p(s^2)$ also follows a power-law behaviour as observed in figure 7(*a*). Taira *et al.* (2016) analysed the network structure of two-dimensional decaying isotropic turbulence and found the undirected node strength (average of in- and out-strength) distribution $p(s)$ to follow a scale-free behaviour if the energy spectrum follows the k^{-3} profile.

For three-dimensional isotropic turbulence, the enstrophy distribution follows a stretched-exponential profile of the form $p(\Omega) \propto \exp(-a_\Omega \Omega^b)$, with a_Ω and b denoting the prefactor and exponent, respectively (Zeff *et al.* 2003; Donzis, Yeung &
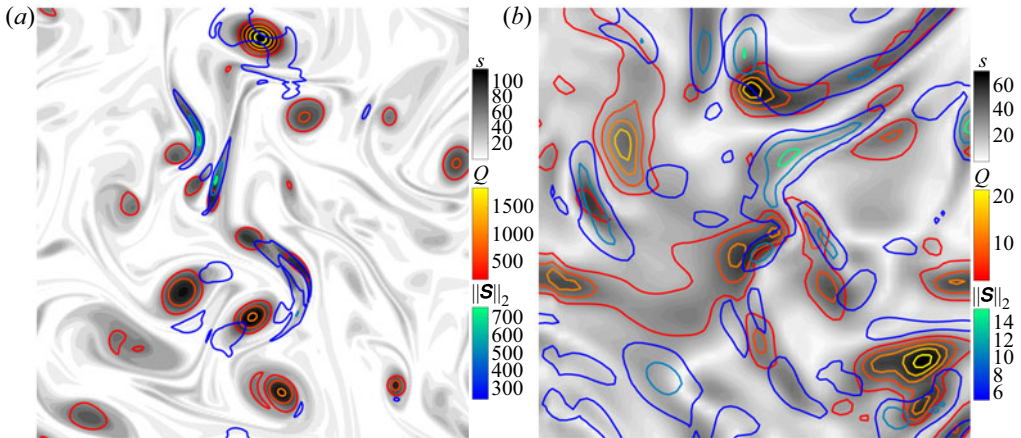
Figure 8. Comparing vortical structures with high node strength (grey contours), Q-criterion (red-yellow contours) and strain (blue-green contours) for (*a*) two- and (*b*) three-dimensional isotropic turbulence. Only a slice is shown for (*b*).

Sreenivasan 2008). We observe a stretched-exponential profile for $p(s^2)$ with the same exponent b as that of the enstrophy distribution, as shown in figure 7(*b*). The difference of $p(s^2)$ for two- and three-dimensional flows can be attributed to the components of vorticity. For three-dimensional turbulence, vorticity is spread over wide scales of structures due to vortex stretching and tilting, which are absent in two-dimensional flows.

The node strength distributions can be used to highlight vortical elements with high node strength, as shown in figure 8. Isocontours of node strength, positive Q-criterion and magnitude of strain rate tensor $\|\boldsymbol{S}\|_2$, for the two- and three-dimensional flow fields are shown. For both flows, the high node strength regions align with those of high positive Q-criterion (vortex core) and $\|\boldsymbol{S}\|_2$ (high shear regions). The node strength-enstrophy relation attributes to the alignment of the node strength with the Q and $\|\boldsymbol{S}\|_2$ measures in physical space. The observations show that the network-based node strength can indeed identify strong vortex cores and shear layers in turbulent flows.

Let us now use the community-based framework to extract vortical communities in isotropic turbulence and identify influential regions to modify the flow using inter- and intra-community strength measures. A demonstration of the community detection algorithm and the corresponding P–Z map applied to a three-dimensional flow field are shown in figure 9(*a*,*b*). Here, the initial community detection procedure coarsely identifies regions in the flow field. The flow field portrayed in figure 9(*a*) only shows regions of high vorticity above a vorticity threshold, ω_{th}. A clear distinction between connectors and peripherals is not observed using the P–Z map. The continuous nature of the flow field and vortical structures being spatially close to each other can make it challenging for the community detection algorithm to extract distinct vortical structures. Similar observations were made in a previous study for laminar wakes (Gopalakrishnan Meena *et al.* 2018). The analysis of complex problems, such as turbulence through network science tools, requires providing physical intuitions to the network-based tools. A naive use of network-theoretic techniques may not necessarily reveal interaction-based characteristics of such complex systems since turbulent flows possess dense networks which are significantly different from most networks studied in network science.

We aid the community detection algorithm by decomposing the flow field into nodes with $Q > 0$ and $Q < 0$. This is portrayed in figure 9(*c*). The communities are identified
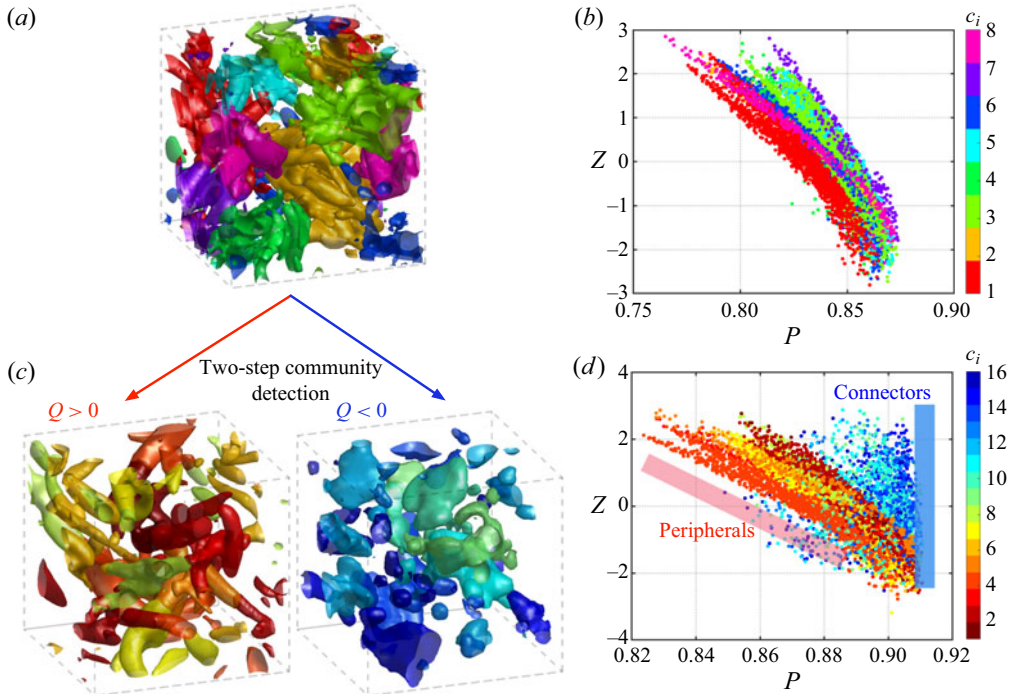
Figure 9. (*a*) Community detection in a three-dimensional isotropic turbulence and (*b*) the corresponding *P–Z* map. (*c*) Two-step community detection and (*d*) the corresponding *P–Z* map. Connector and peripheral communities have distinct distributions in the *P–Z* map.

independently for the two networks. The difference in the number of communities compared with the first step is due to the value of γ_M used, which was found to be similar for both the steps for the given Re_λ. The new community labels are used to evaluate the *P–Z* map for the full adjacency matrix, as shown in figure 9(*d*). The two-step community detection procedure reveals the communities to broadly follow two correlations in the *P–Z* map. The communities on the left side of the map possess a negative correlation in the *P–Z* feature space and the nodes on the left side exhibit no significant correlation. We classify the former as peripheral and later as connector communities. The first group predominantly contains nodes with $Q > 0$, the second group with $Q < 0$. Thus, most peripheral and connector communities resemble vortex-core and shear-layer-type structures, respectively. Vortex cores that are spatially isolated in the flow can attribute to their classification as peripherals. Whereas, most shear-layer-type structures being located amongst vortical structures make them connectors. We observe similar results for two-dimensional isotropic turbulence and for other cases at various Re_λ. Given the classification of vortical structures into connector and peripheral communities, we can now identify the important communities and analyse their influence on the flow field.

4.3. *Community-based flow modification*

We compute the $\overline{P_k}$ of each community k to quantify the strength of influence. The connector and peripheral communities are the ones with $\max_k \overline{P_k}$ and $\min_k \overline{P_k}$, respectively, as highlighted in figure 10(*a*). The dominant nodes of the communities are determined based on Z. The peripheral community corresponds to the vortical structure
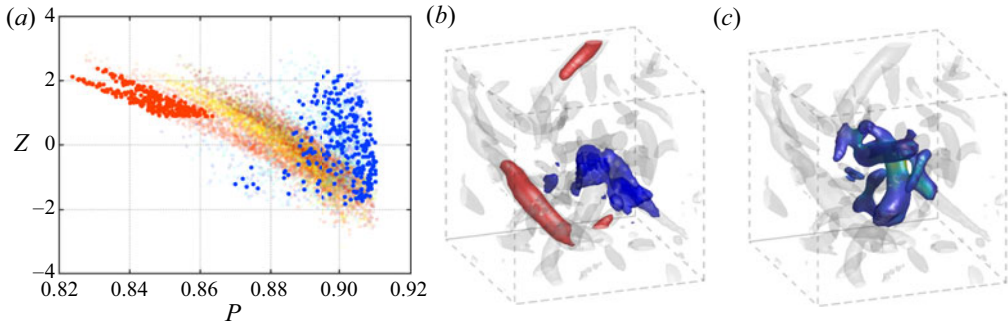
Figure 10. (*a*) Identification of the connectors and peripherals in the *P–Z* map and (*b*) their structures in physical space. The red and blue colours denote the vortical structures corresponding to the strongest peripheral and connector communities, respectively. The transparent grey isosurfaces of *Q*-criterion represent the background flow field (vortical cores) for reference. (*c*) Local region around the connector structure, which is one integral length scale around the centroid of the structure.

visualized in red and the connector community comprising low circulation multivortical structures with both strain and rotational regions visualized in blue in figure 10(*b*).

We compare the influence of the connector structure to modify the flow with the strongest vortex tube and shear-layer-based regions, which are known to cause many flow modifications. The vortex tube and shear-layer structures are identified by large amplitudes of $Q > 0$ and $Q < 0$, respectively. Herein, notations Q^+ and Q^- are correspondingly used to denote the strongest vortex tube and shear-layer structures in the flow field. We do not present cases for the peripheral structures as they usually align with Q^+.

We add perturbations to the nodes identified as influential structures and track the changes to the flow. Impulse perturbations at discrete time $n_t \Delta t$ are added to the velocity field with time step Δt and $n_t = 0, 1, 2, \ldots$. The perturbed velocity field at time t is given by $u(r, t) + \tilde{u}(r, r^*, t)$, where $\tilde{u}(r, r^*, t) = \alpha \tilde{f}(r, r^*, t)$, α is the amplitude of the perturbation added to the perturbation $\tilde{f}(r, r^*, t)$ and r^* is the location of the influential structure. The perturbation is given by

$$f(r, r^*, t) = \frac{\hat{e}_{u(r,t)}}{\sqrt{2\pi \Delta V^2}} \sum_{i=1}^{n_p} \exp\left(\frac{-\|r - r_i^*\|_2^2}{2\Delta V^2}\right) \delta(t - n_t \Delta t), \qquad (4.2)$$

where $\hat{e}_{u(r,t)}$ is the unit vector in the direction of $u(r, t)$, ΔV is the volume of the vortical node (grid size) and r_i^* are the locations of all the n_p perturbed nodes of the influential structure. We normalize $f(r, r^*, t)$ to give $\tilde{f}(r, r^*, t)$ such that $\int_V \|\tilde{f}(r, r^*, t)\|_2^2 \, dV = 1$. A prescribed forcing energy E of

$$E = \frac{\int_V \|\tilde{u}(r, r^*, t)\|_2^2 \, dV}{\int_V \|u(r, t)\|_2^2 \, dV} \qquad (4.3)$$

is used to compute the amplitude of perturbation α.

We first analyse the influence of the structures with a single perturbation added to all the nodes of the influential structures at the initial time instant. The perturbation amplitude is chosen such that $E = 0.04$, which is a reasonable magnitude for control. Based on the observations, we then employ multiple pulses to the nodes of the influential structures at

915 A10-16

time periodic instances $n_t \Delta t$. These influential structures are tracked in time for given isocontours (or isosurfaces) of Q-criterion and are subjected to impulse perturbations with time step normalized by the large eddy turn-overtime at the initial time instant, $\Delta t / \tau_e(t_0) = 1$ and 0.2 for two- and three-dimensional flows, respectively. We have chosen the time step for these turbulent flows based on the single perturbation analysis to obtain significant flow modification. The difference in time step for two- and three-dimensional isotropic turbulence is to consider the distinct predictability horizon of small-scale motion in the flows (Métais & Lesieur 1986; Lesieur & Métais 1996; Machiels 1997). While the two-dimensional flow would have predictability horizons spanning over a few eddy turn-over times, the present three-dimensional flow has a shorter time horizon. Herein, we refer to the experiments with perturbations at the initial time instant and multiple pulses at time periodic instances as single and multiple perturbations, respectively.

We concentrate on the flow evolution cases in the vicinity of the perturbed structures, one integral length scale around the centroid of the perturbed structure, as shown in figure 10(c). The peripheral-based or Q^+ perturbations increase the circulation of the vortex core. In contrast, modification of the behaviour of multiple vortical structures by the connector-based and Q^- perturbations enhances local mixing in the flow, as we discuss below. Based on the observations from the present study (for which the influential structures are identified only at the initial time instant), we have also performed preliminary analyses with the structure identification procedure repeated as the flow evolves. We observe similar results showing perturbation of the connector structures significantly enhancing turbulent mixing compared with perturbing Q^+ and Q^- structures. In the present study, we concentrate on the structures identified at the initial time instant to characterize the influence of the network-based structures on turbulence.

Mixing enhancement in turbulent flows plays a key role in various engineering applications. Mixing enhancement by stirring has been attributed to generation of shear dominated filaments in the flow field (Spencer & Wiley 1951; Aref 1984; Ottino 1990; Eggl & Schmid 2018). Here, we analyse the effect of the perturbations to enhance local mixing in isotropic turbulence based on the present network-based framework. We use fluid-particle tracking to quantify local mixing in the flow field. To quantify mixing, we consider the use of two-species fluid tracking (Coppola, Sherwin & Peiró 2001). The first species is initialized one integral length scale around the centroid of the perturbed structure, the region previously shown in figure 10(c), and the second over the rest of the flow field. Given the velocity field $\boldsymbol{u}(\boldsymbol{r}, t)$, the time evolution of the fluid particle at $\boldsymbol{r}_p$ is given by

$$\frac{\mathrm{d}\boldsymbol{r}_p}{\mathrm{d}t} = \boldsymbol{u}(\boldsymbol{r}_p, t). \tag{4.4}$$

A second-order accurate Runge–Kutta scheme is implemented for time integration (Yu *et al.* 2012).

Local mixing is quantified by measuring the information entropy using the two species of particles in the domain (Kang & Kwon 2004; Cookson, Doorly & Sherwin 2019). The flow field is discretized into cells and the entropy of the two species of particles is evaluated for each cell. The total information entropy of the whole domain at an instant in time is given by

$$S = -\sum_{i=1}^{n_c} \left[w_i \sum_{k=1}^{2} (n_{i,k} \log n_{i,k}) \right], \tag{4.5}$$

where n_c is the number of cells with which the full domain is discretized, $n_{i,k}$ is the number of particles of kth species in ith cell and w_i is the weight factor. If the ith cell contains no
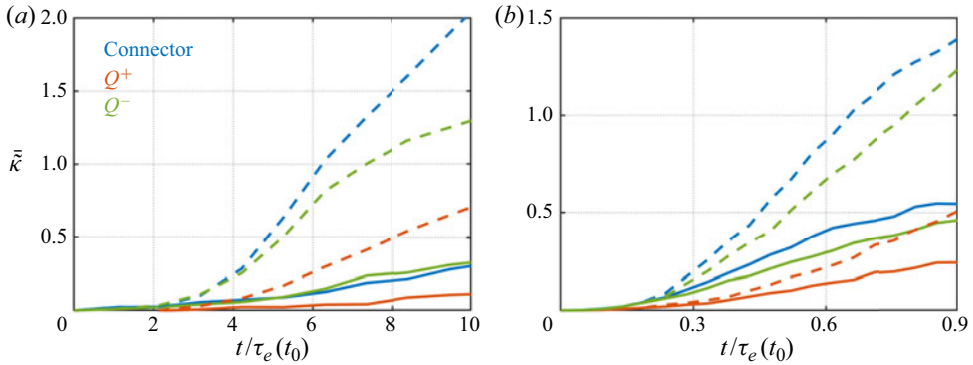
Figure 11. Ensemble average of normalized relative particle entropy in time for (*a*) two- and (*b*) three-dimensional isotropic turbulent flows subjected to connector-based, Q^+, and Q^- perturbations. Lines — denote results for single perturbation and −− for multiple perturbation cases. Ensemble is computed using 10 cases.

particles or only particles of a single species, $w_i = 0$, else $w_i = 1$. Moreover, the relative entropy measure κ (Kang & Kwon 2004) is given by

$$\kappa(t) = \frac{S(t) - S(t_0)}{S_{max} - S(t_0)},\tag{4.6}$$

where $S(t_0)$ is the entropy for initial particle distribution and S_{max} is the maximum possible entropy increase over the domain, which is achieved when each cell contains equal number of particles of each species. For each perturbation set-up, we normalize κ by the baseline κ_{base} as $\tilde{\kappa}(t) = [\kappa(t) - \kappa_{base}(t)]/\|\kappa_{base}(t)\|_\infty$, thus measuring the mixing enhancement compared with the baseline flow. The baseline flow field is initialized with particles in the same pattern as each perturbed simulation to evaluate the respective κ_{base}.

Ensemble averages of $\tilde{\kappa}$ for connector, Q^+, and Q^--based perturbations performed on a number of two- and three-dimensional isotropic turbulent flows are shown in figure 11. For the two-dimensional isotropic turbulence with a single perturbation at the initial time instant, the connector-based perturbation achieves mixing enhancement similar to that of Q^-. Both connector-based and Q^- perturbations outperform Q^+ for local mixing enhancement. With multiple pulses, connector-based perturbation generates entropy two times compared with the baseline flow, which is 54 % more than the Q^- perturbations. The perturbation using Q^+ just leads to strengthening of vortex cores without significant spreading of particles, which will be visualized shortly.

Using the results of two-dimensional flows as a guideline, we perform the analysis on three-dimensional flows, as shown in figure 11(*b*). A single pulse added to the connector at the initial time instant generates $\tilde{\kappa}$ values 0.55 times that of the baseline flow, which is 20 % more than the Q^- perturbation. With multiple pulses, connector-based perturbations increase the entropy by 1.4 times compared with the baseline flow, which is 17 % more than the Q^- perturbations. Multiple pulses of Q^+ perturbation under-performs compared with even the single connector-based perturbation. According to the studies on mixing enhancement using stirrers (Aref 1984; Eggl & Schmid 2018), we expect the Q^- perturbation to achieve better mixing. The present results are in agreement with these studies. Moreover, the connector-based perturbation outperforms the Q^- perturbation, highlighting the capability of the network-theoretic framework to identify structures to effectively modify the flow.
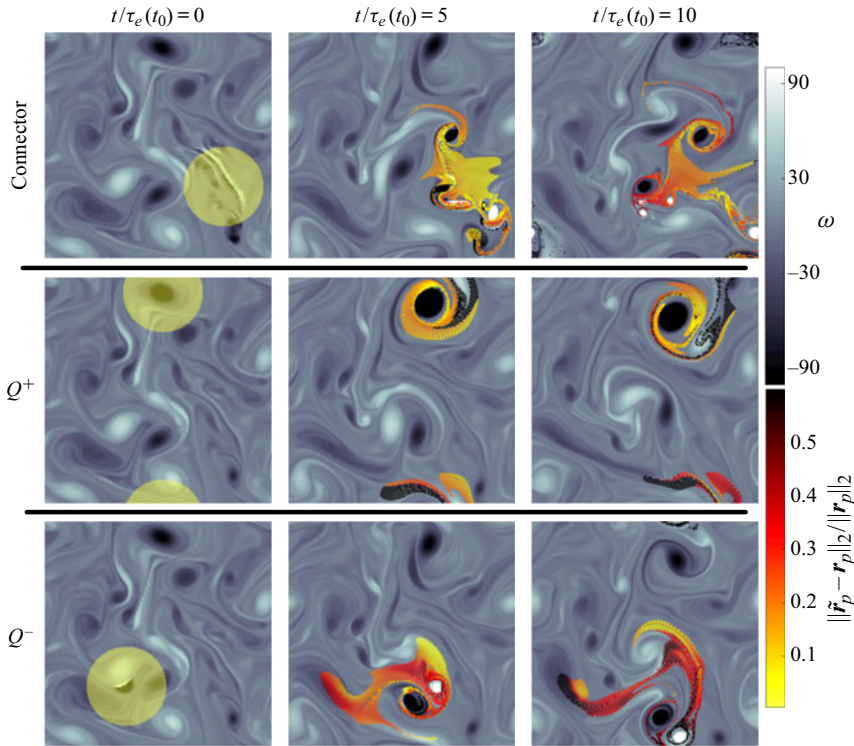
915 A10-18

Figure 12. Time evolution of a two-dimensional isotropic turbulent flow subjected to multiple perturbations. Fluid tracers initialized around the perturbation are coloured by the change in trajectory with perturbation $\tilde{r}_p$ compared with the corresponding baseline trajectory r_p.

With the above observations quantifying the effectiveness of connectors to modify turbulence and enhance local turbulence mixing, let us analyse the flow fields. We consider the time evolution of a two-dimensional isotropic decaying turbulent flow subject to multiple pulses of connector-based, Q^+, and Q^- perturbations, as shown in figure 12. The flow field is visualized using vorticity ω. The fluid particle species initialized one integral length around the perturbation is also shown. The yellow–red colour gradient represents the amount of change in trajectories compared with the corresponding baseline trajectory. A uniform colour distribution indicates effective mixing. The connector-based perturbation achieves the narrowest range in colour distribution at the final instant. While Q^+ and Q^- perturbations achieve higher magnitudes of change in trajectories for certain particles, highlighted in black, some particles are spread out least, as highlighted in bright yellow.

Multiple pulses on the Q^+ structure strengthens the vortex core, making a large distinct vortex. The tracers rotate around the vortex core due to the vorticity. Only the tracers at the boundary of the vortex are spread out significantly. The Q^- perturbation, comprising the strained region between the vortex-dipoles, forms a jet-like flow. With multiple perturbations, the jet-like flow spreads the tracers more effectively compared with that achieved in the baseline and Q^+ perturbations. These observations are in agreement with recent findings that vortex-dipole-like structures in two-dimensional isotropic turbulence promote effective flow modification (Jiménez 2020; Yeh *et al.* 2021). The connector structures comprise a long shear-layer-type vortical structure and near-by vortices of
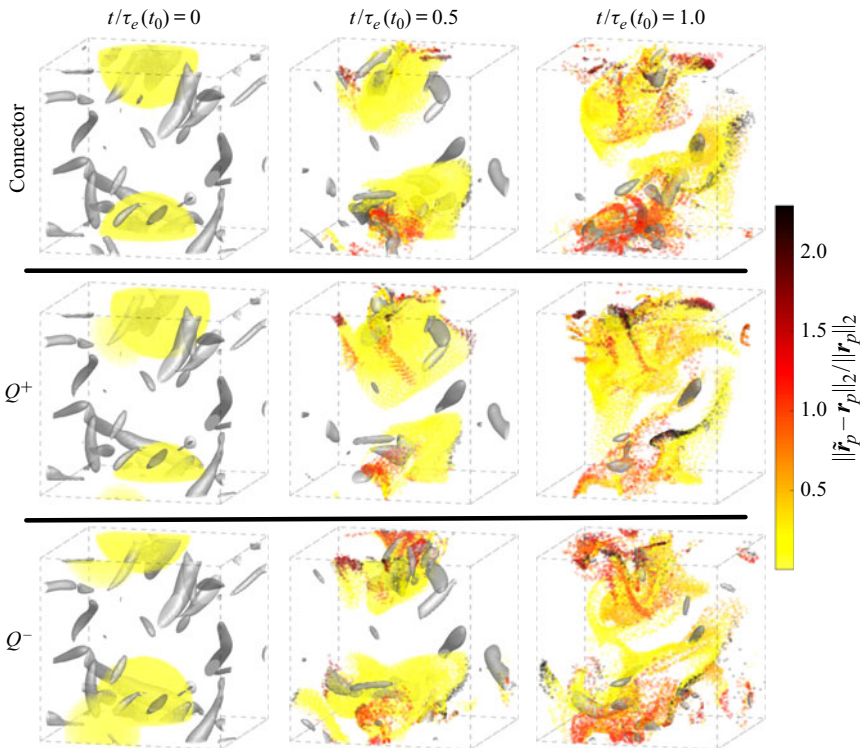
Figure 13. Time evolution of a three-dimensional isotropic turbulent flow subjected to multiple perturbations. Vortical structures are depicted by isosurface of Q-criterion. Fluid tracers initialized around the perturbation are coloured by the change in trajectory with perturbation $\tilde{r}_p$ compared with the corresponding baseline trajectory r_p.

low vorticity. Multiple perturbations of the shear-layer-type structure lead to the formation of small-scale vortices, which enhances flow mixing compared with the baseline, as well as Q^+ and Q^- perturbations.

The evolution of particle tracers in a three-dimensional turbulent flow subjected to multiple perturbations on connector, Q^+, and Q^- structures are presented in figure 13. Here, the Q^+, Q^- and connector structures are spatially located close to each other at the initial time instant. The flow field at the final instant corresponding to connector-based perturbation has the narrowest range in colour distribution of the tracers, depicting highest mixing enhancement. The broadest range in colour distribution corresponds to Q^+ perturbation, which denotes the least mixing enhancement achieved. Multiple pulses of connector-based perturbations lead to the generation of small-scale structures. On the other hand, the vortical structures decay in time with Q^+ and Q^- perturbations.

Next, let us examine the local flow region around the perturbation to analyse the effect of the network-based connector to modify its neighbouring vortical structures. We analyse the time evolution of the local flow region around the connector, Q^+, and Q^- structures, as presented in figure 14. The vortical structures are tracked using the isosurface of Q-criterion, with a constant value of Q in time. A single pulse is added to the connector, Q^+, and Q^- structures at the initial time instant. The perturbed structures at the initial time instant are shown on the left column, visualized by the green isosurfaces. The neighbouring vortex tubes under consideration in each case (row) are depicted by the
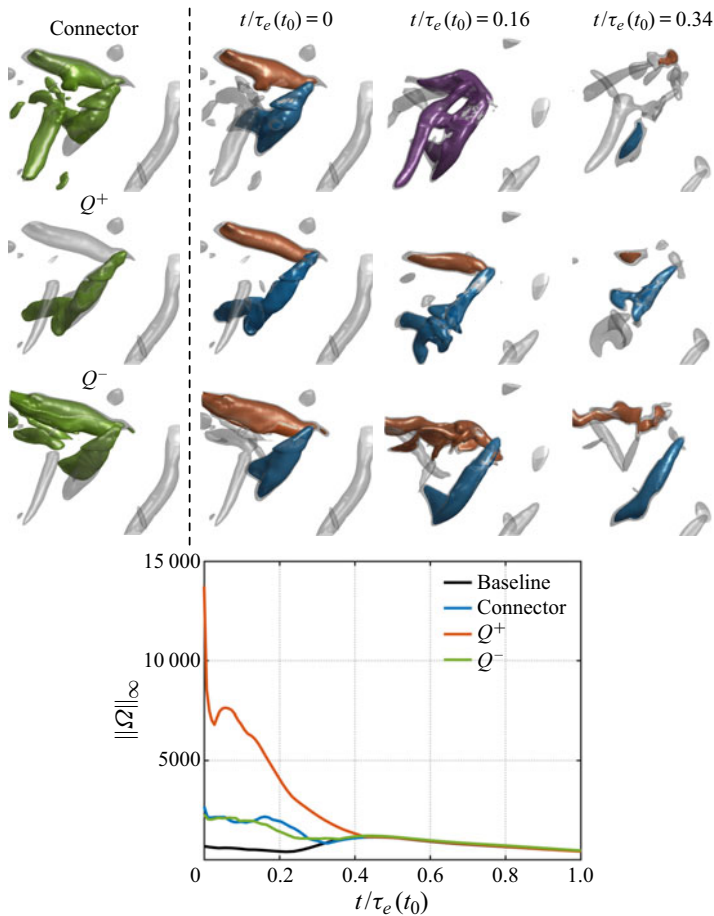
Figure 14. Modification of two vortex tubes in a three-dimensional isotropic turbulent flow using connector-based, Q^+, and Q^- perturbations. The vortical structures are visualized by the isosurface of Q-criterion, with a constant value of Q in time. The green, blue and red colours of the isosurfaces represent the perturbed structures at the initial time and the two vortex tubes under consideration, respectively. The grey transparent isosurface denotes the background flow field for each case. The connector effectively modifies both the vortex cores as shown using the isosurface of Q-criterion and local growth of maximum enstrophy $\|\Omega\|_\infty$ between time $t/\tau_e(0) = 0.12$ and 0.2.

blue and red isosurface. The growth of maximum enstrophy, $\|\Omega\|_\infty$, is also evaluated to observe modification of the vortex cores (Foias & Temam 1989; Ayala & Protas 2017). We note that at time $t/\tau_e(0) = 0.34$, the connector structure leads to modification of both the neigboring vortex tubes and formation of smaller-scale structures. These small-scale structures induce enhanced local spreading of the fluid particles, as observed in figure 13.

Perturbation of the Q^+ structure (shown in blue) leads to the increase in circulation of the vortex core and eventual breakup of the blue isosurface at time $t/\tau_e(0) = 0.16$. The modification of the Q^+ structure is also observed by the peak of $\|\Omega\|_\infty$ at $t/\tau_e(0) = 0.05$. The curved geometry of the Q^+ vortex core at the initial time instant may instigate instabilities when perturbation is added, resulting in the significant modification of the vortex core. Nonetheless, the Q^+ perturbation has negligible influence on the neighbouring vortex highlighted in red. Note that these observations are similar to the characteristics of a network-based peripheral structure. The Q^- structure is the strongest shear-layer structure,

915 A10-21

which is located between the two neighbouring vortex tubes. Thus, the Q^- perturbation results in the modification of both the blue and red isosurfaces. Both the vortex cores decay in time with no peaks appearing for $\|\Omega\|_\infty$ over time, suggesting lower modification of the vortex cores achieved by the Q^- structure compared with Q^+ perturbation.

The connector structure comprises the shear-layer region between the two neighbouring vortex tubes and an adjacent vortical structure with low circulation. This adjacent vortical structure merely decays within a short time in the Q^+ and Q^- simulations. With connector-based perturbation, the adjacent vortical structure connects with the two neighbouring vortex tubes through the shear layer, forming one large vortical structure highlighted in purple at time $t/\tau_e(0) = 0.16$. Eventually, the connection results in the significant breakup of both the blue and red isosurfaces, leading to the formation of smaller scales of vortical structures. The observations show the advantage of connectors to modify multiple vortical structures compared with Q^+ perturbations. The local growth of $\|\Omega\|_\infty$ between $t/\tau_e(0) = 0.13$ and 0.2 denotes effective modification of the vortex cores compared with that achieved by Q^- perturbation. The connection amongst the vortical structures, in the form of vorticity, is not aligned with the direction of rotation of the two neighbouring vortex tubes, which may result in instabilities, leading to significant breakup of the vortex cores. The above illustrative examples demonstrate the ability of network-based methodologies to extract vortical structures of low circulation that can effectively influence neighbouring vortical structures in turbulent flows.

5. Concluding remarks

A network community-based formulation was introduced to extract flow-modifying vortical structures in two- and three-dimensional isotropic turbulence. The network framework considered the vortical elements in a flow as nodes of a vortical interaction network (graph). The web of interactions amongst the vortical elements was quantified by the induced velocity, which was assigned to the weighted network edges. This interaction-based framework was used to identify groups of closely connected vortical nodes, called communities. The interactions amongst these communities were used to identify the most influential community which can modify the system dynamics significantly. Taking advantage of the inter-community interactions, we showed that local turbulent mixing can be enhanced using vortical structures attributed with low circulation. The goal of this network-based framework was not to alter the global turbulent flow, but influence certain key vortical structures under the settings of isotropic turbulence.

We use the community characteristics to extract the inter- and intra-community interactions amongst groups of vortical nodes. The strengths of these interactions were used to identify the connector and peripheral nodes, which have the highest and least influence on other communities, respectively. The node with the maximum total interaction strength was identified as the hub. The ability of these influential nodes to modify the networked dynamics was demonstrated on a model fluid flow of a collection of discrete point vortices. Impulse velocity perturbations were added to the connector, peripheral and hub communities identified at the initial time instant. The connector community effectively modified trajectories of the other communities compared with the hub and peripheral-based perturbations. We then applied the community-based formulations to identify influential structures in two- and three-dimensional isotropic turbulence. The connector and peripheral structures were found to resemble shear-layer and vortex-core-type structures, respectively. Adding perturbations to the connector

structures, which have low vorticity, led to enhanced local flow mixing compared with the effect of perturbing the strongest shear layer and vortex tube.

The present demonstrations of the network-based formulation on isotropic turbulence modification encourage the future extensions of the present framework on flows of practical interest. Within the current work, we have not considered the necessary computational effort for performing the network-based analysis. However, there are emerging network-based characterization (Bai *et al.* 2019) and modelling techniques (Nair & Taira 2015) for fluid flows that can be leveraged to perform the present analysis with reduced computational resource. Moreover, the decomposition of the governing equation for a networked system using the inter- and intra-community interactions can be extended to community-based reduced-order modelling efforts for complex flows (Gopalakrishnan Meena *et al.* 2018). Based on these frameworks and extensions, the present characterization and open-loop control offers a pathway for future modelling and advanced flow control efforts to modify the dynamics of vortical structures in a complex turbulent flow field.

Author ORCIDs.
Ⓘ Muralikrishnan Gopalakrishnan Meena https://orcid.org/0000-0003-4048-4639;
Ⓘ Kunihiko Taira https://orcid.org/0000-0002-3762-8075.

Appendix. Reynolds number and dimension reduction independence of network measures

We assess the effect of Reynolds number on the network representation of vortical interactions in isotropic turbulence by evaluating the node strength distribution for three-dimensional flow fields with various Re_λ, as shown in figure 15(*a*). The strength distributions of flows with different Reynolds numbers collapse to a single curve with the use of appropriate non-dimensionalization for the edge weights. The results suggest that the network formulation is able to capture the key characteristics of the universal scaling of isotropic turbulence. The fine resolution of spatial discretization required to simulate turbulent flows also poses a challenge to analyse the interactions amongst the vortical elements. We subsample the flow field to reduce the dimension of the flow field being analysed.

The effect of subsampling the turbulent flow field on the network measures is evaluated by comparing the node strength distribution of various low-resolution flow fields. A three-dimensional flow field of $Re_\lambda = 40$ with a grid resolution of $256 \times 256 \times 256$ is used. We subsample the data to various smaller grid resolutions and compute the node strengths, as shown in figure 15(*b*). The node strength computed based on the non-dimensionalized edge weight allows scaling of the distributions. The node strength distributions collapse into a single distribution and converge with higher grid resolution. The k_{max} for each low-resolution grid used in the node strength distribution computation is depicted in the energy spectra in figure 15(*c*). The grid resolution using a $64 \times 64 \times 64$
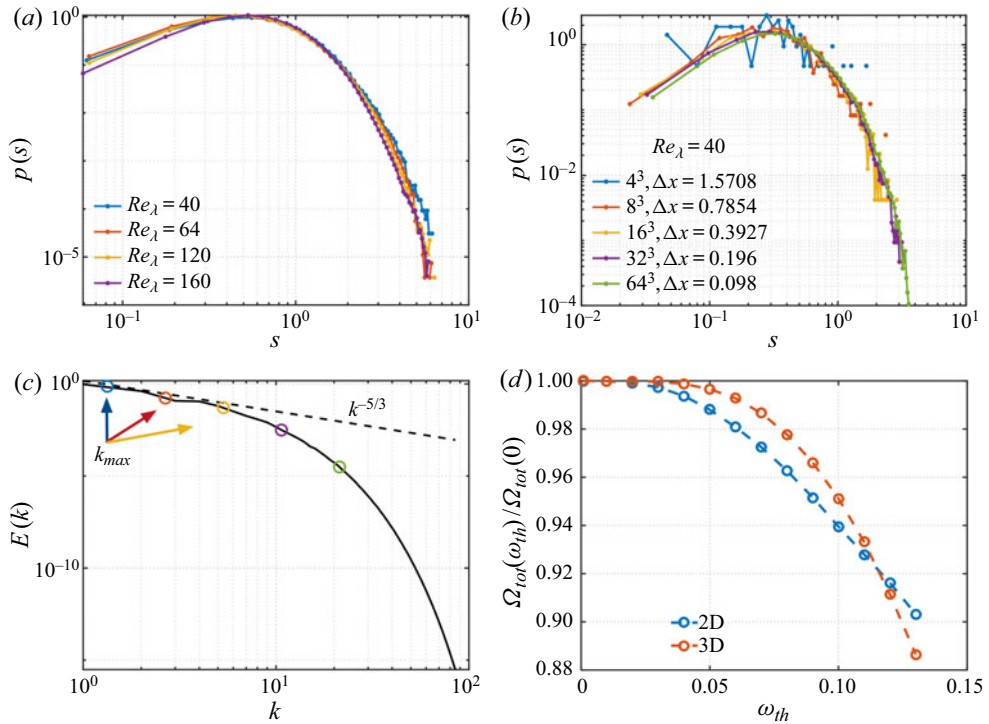
Figure 15. (*a*) Collapse of node strength distribution with increase in Reynolds number. (*b*) Convergence of node strength distribution over sampling rate in three-dimensional turbulence at $Re_\lambda = 40$. (*c*) Maximum resolvable wavenumber for various grid resolution or sampling rate. (*d*) Variation of total enstrophy Ω_{tot} with vorticity threshold for two- and three-dimensional turbulence.

grid satisfies the $k_{max}\eta \geqslant 1$ condition. The results also demonstrate the application of network-based formulation from a discrete to continuous description of the flow field.

We only analyse vortical elements in the flow field with high vorticity, extracted through vorticity threshold. The choice of the vorticity threshold of $\omega_{th} = 0.05||\boldsymbol{\omega}(\boldsymbol{r})||_\infty$ is given by analysing the effect of thresholding on the total enstrophy of the flow field Ω_{tot} (following (4.1)), as shown in figure 15(*d*). For both two- and three-dimensional turbulence, $\omega_{th} = 0.05||\boldsymbol{\omega}(\boldsymbol{r})||_\infty$ results in retaining more than 98 % of the total enstrophy of the original flow field, $\Omega_{tot}(\omega_{th} = 0)$. This is similar to the values used to analyse structures of high vorticity (Jiménez *et al.* 1993; Moisy & Jiménez 2004), capturing the influential regions of the flow.

REFERENCES

ALBERT, R., JEONG, H. & BARABÁSI, A.-L. 2000 Error and attack tolerance of complex networks. *Nature* **406**, 378–382.

AREF, H. 1984 Stirring by chaotic advection. *J. Fluid Mech.* **143**, 1–21.

AREF, H. 2007 Point vortex dynamics: a classical mathematics playground. *J. Math. Phys.* **48** (6), 065401.

AYALA, D. & PROTAS, B. 2017 Extreme vortex states and the growth of enstrophy in three-dimensional incompressible flows. *J. Fluid Mech.* **818**, 772–806.

BAI, Z., ERICHSON, N.B., GOPALAKRISHNAN MEENA, M., TAIRA, K. & BRUNTON, S.L. 2019 Randomized methods to characterize large-scale vortical flow networks. *PLoS One* **14** (11), e0225265.

BARABÁSI, A.-L. 2016 *Network Science*. Cambridge University Press.

BENZI, R., PATARNELLO, S. & SANTANGELO, P. 1987 On the statistical properties of two-dimensional decaying turbulence. *Europhys. Lett.* **3** (7), 811.

BHATTACHARJEE, S., SCHEELKE, B. & TROUTT, T.R. 1986 Modification of vortex interactions in a reattaching separated flow. *AIAA J.* **24** (4), 623–629.

BLONDEL, V.D., GUILLAUME, J.-L., LAMBIOTTE, R. & LEFEBVRE, E. 2008 Fast unfolding of communities in large networks. *J. Stat. Mech.* **2008** (10), P10008.

BOLLOBÁS, B. 1998 *Modern Graph Theory*. Springer.

BOLLT, E.M. 2001 Combinatorial control of global dynamics in a chaotic differential equation. *Intl J. Bifurcation Chaos* **11** (08), 2145–2162.

BRACHET, M.E., MENEGUZZI, M. & SULEM, P.L. 1986 Small-scale dynamics of high-Reynolds-number two-dimensional turbulence. *Phys. Rev. Lett.* **57** (6), 683.

BRUNTON, S.L. & NOACK, B.R. 2015 Closed-loop turbulence control: progress and challenges. *Appl. Mech. Rev.* **67** (5), 050801.

CHAKRABORTY, P., BALACHANDAR, S. & ADRIAN, R.J. 2005 On the relationships between local vortex identification schemes. *J. Fluid Mech.* **535**, 189–214.

CHUMAKOV, S.G. 2008 A priori study of subgrid-scale flux of a passive scalar in isotropic homogeneous turbulence. *Phys. Rev.* E **78** (3), 036313.

COOKSON, A.N., DOORLY, D.J. & SHERWIN, S.J. 2019 Efficiently generating mixing by combining differing small amplitude helical geometries. *Fluids* **4** (2), 59.

COPPOLA, G., SHERWIN, S.J. & PEIRÓ, J. 2001 Nonlinear particle tracking for high-order elements. *J. Comput. Phys.* **172** (1), 356–386.

DONZIS, D.A., YEUNG, P.K. & SREENIVASAN, K.R. 2008 Dissipation and enstrophy in isotropic turbulence: resolution effects and scaling in direct numerical simulations. *Phys. Fluids* **20** (4), 045108.

DUBIEF, Y. & DELCAYRE, F. 2000 On coherent-vortex identification in turbulence. *J. Turbul.* **1**, N11.

EGGL, M.F. & SCHMID, P.J. 2018 A gradient-based framework for maximizing mixing in binary fluids. *J. Comput. Phys.* **368**, 131–153.

FOIAS, C. & TEMAM, R. 1989 Gevrey class regularity for the solutions of the Navier–Stokes equations. *J. Funct. Anal.* **87** (2), 359–369.

FORTUNATO, S. 2010 Community detection in graphs. *Phys. Rep.* **486** (3), 75–174.

FORTUNATO, S. & BARTHÉLEMY, M. 2007 Resolution limit in community detection. *Proc. Natl Acad. Sci. USA* **104** (1), 36–41.

GODAVARTHI, V., UNNI, V.R., GOPALAKRISHNAN, E.A. & SUJITH, R.I. 2017 Recurrence networks to study dynamical transitions in a turbulent combustor. *Chaos* **27** (6), 063113.

GOPALAKRISHNAN MEENA, M. 2020 Network community-based analysis of complex vortical flows: laminar and turbulent flows. PhD thesis, University of California, Los Angeles, CA, USA.

GOPALAKRISHNAN MEENA, M., NAIR, A.G. & TAIRA, K. 2018 Network community-based model reduction for vortical flows. *Phys. Rev.* E **97**, 063103.

GRAFTIEAUX, L., MICHARD, M. & GROSJEAN, N. 2001 Combining PIV, POD and vortex identification algorithms for the study of unsteady turbulent swirling flows. *Meas. Sci. Technol.* **12** (9), 1422–1429.

GUIMERA, R. & AMARAL, L.A.N. 2005 Functional cartography of complex metabolic networks. *Nature* **433** (7028), 895–900.

GUIMERA, R., MOSSA, S., TURTSCHI, A. & AMARAL, L.A.N. 2005 The worldwide air transportation network: anomalous centrality, community structure, and cities' global roles. *Proc. Natl Acad. Sci. USA* **102** (22), 7794–7799.

GÜRCAN, Ö.D. 2017 Nested polyhedra model of turbulence. *Phys. Rev.* E **95** (6), 063102.

GÜRCAN, Ö.D. 2018 Nested polyhedra model of isotropic magnetohydrodynamic turbulence. *Phys. Rev.* E **97** (6), 063111.

GÜRCAN, Ö.D., LI, Y. & MOREL, P. 2020 Turbulence as a network of Fourier modes. *Mathematics* **8** (4), 530.

HADJIGHASEM, A., KARRASCH, D., TERAMOTO, H. & HALLER, G. 2016 Spectral-clustering approach to Lagrangian vortex detection. *Phys. Rev.* E **93** (6), 063107.

HALLER, G. 2005 An objective definition of a vortex. *J. Fluid Mech.* **525**, 1–26.

HALLER, G. 2015 Lagrangian coherent structures. *Annu. Rev. Fluid Mech.* **47**, 137–162.

HUNT, J.C.R., WRAY, A.A. & MOIN, P. 1988 Eddies, stream, and convergence zones in turbulent flows. *Tech. Rep.* CTR-S88. Center for Turbulence Research.

HUSIC, B.E., SCHLUETER-KUCK, K.L. & DABIRI, J.O. 2019 Simultaneous coherent structure coloring facilitates interpretable clustering of scientific data by amplifying dissimilarity. *PLoS One* **14** (3), e0212442.

HUSSAIN, A.K.M.F. 1986 Coherent structures and turbulence. *J. Fluid Mech.* **173**, 303–356.

IACOBELLO, G., MARRO, M., RIDOLFI, L., SALIZZONI, P. & SCARSOGLIO, S. 2019*a* Experimental investigation of vertical turbulent transport of a passive scalar in a boundary layer: statistics and visibility graph analysis. *Phys. Rev. Fluids* **4** (10), 104501.

IACOBELLO, G., SCARSOGLIO, S., KUERTEN, J.G.M. & RIDOLFI, L. 2018*a* Spatial characterization of turbulent channel flow via complex networks. *Phys. Rev.* E **98** (1), 013107.

IACOBELLO, G., SCARSOGLIO, S., KUERTEN, J.G.M. & RIDOLFI, L. 2019*b* Lagrangian network analysis of turbulent mixing. *J. Fluid Mech.* **865**, 546–562.

IACOBELLO, G., SCARSOGLIO, S. & RIDOLFI, L. 2018*b* Visibility graph analysis of wall turbulence time-series. *Phys. Lett.* A **382** (1), 1–11.

JEONG, J. & HUSSAIN, F. 1995 On the identification of a vortex. *J. Fluid Mech.* **285**, 69–94.

JIMÉNEZ, J. 2018 Machine-aided turbulence theory. *J. Fluid Mech.* **854**, R1.

JIMÉNEZ, J. 2020 Monte Carlo science. *J. Turbul.* **21** (9–10), 544–566.

JIMÉNEZ, J., WRAY, A.A., SAFFMAN, P.G. & ROGALLO, R.S. 1993 The structure of intense vorticity in isotropic turbulence. *J. Fluid Mech.* **255**, 65–90.

KANG, T.G. & KWON, T.H. 2004 Colored particle tracking method for mixing analysis of chaotic micromixers. *J. Micromech. Microengng* **14** (7), 891–899.

KIDA, S. 1985 Numerical simulation of two-dimensional turbulence with high-symmetry. *J. Phys. Soc. Japan* **54** (8), 2840–2854.

KRISHNAN, A., MANIKANDAN, R., MIDHUN, P.R., REEJA, K.V., UNNI, V.R., SUJITH, R.I., MARWAN, N. & KURTHS, J. 2019*a* Mitigation of oscillatory instability in turbulent reactive flows: a novel approach using complex networks. *Europhys. Lett.* **128** (1), 14003.

KRISHNAN, A., SUJITH, R.I., MARWAN, N. & KURTHS, J. 2019*b* On the emergence of large clusters of acoustic power sources at the onset of thermoacoustic instability in a turbulent combustor. *J. Fluid Mech.* **874**, 455–482.

KRUEGER, P.S., HAHSLER, M., OLINICK, E.V., WILLIAMS, S.H. & ZHARFA, M. 2019 Quantitative classification of vortical flows based on topological features using graph matching. *Proc. R. Soc. Lond.* A **475** (2228), 20180897.

KUNDU, P.K., COHEN, I.M. & DOWLING, D.R. 2011 Velocity induced by a vortex filament: law of Biot and Savart. In *Fluid Mechanics*, chap. 5, pp. 181–183. Academic Press.

LEICHT, E.A. & NEWMAN, M.E.J. 2008 Community structure in directed networks. *Phys. Rev. Lett.* **100** (11), 118703.

LESIEUR, M. & METAIS, O. 1996 New trends in large-eddy simulations of turbulence. *Annu. Rev. Fluid Mech.* **28** (1), 45–82.

LUMLEY, J.L. 1967 The structure of inhomogeneous turbulent flows. In *Atmospheric Turbulence and Radio Wave Propagation* (ed. A.M. Yaglam & V.I. Tatarsky), pp. 166–177. Nauka.

MACHIELS, L. 1997 Predictability of small-scale motion in isotropic fluid turbulence. *Phys. Rev. Lett.* **79** (18), 3411.

MCWILLIAMS, J.C. 1984 The emergence of isolated coherent vortices in turbulent flow. *J. Fluid Mech.* **146**, 21–43.

MÉTAIS, O. & LESIEUR, M. 1986 Statistical predictability of decaying turbulence. *J. Atmos. Sci.* **43** (9), 857–870.

MOISY, F. & JIMÉNEZ, J. 2004 Geometry and clustering of intense structures in isotropic turbulence. *J. Fluid Mech.* **513**, 111–133.

MURAYAMA, S., KINUGAWA, H., TOKUDA, I.T. & GOTODA, H. 2018 Characterization and detection of thermoacoustic combustion oscillations based on statistical complexity and complex-network theory. *Phys. Rev.* E **97** (2), 022223.

NAIR, A.G., BRUNTON, S.L. & TAIRA, K. 2018 Networked-oscillator-based modeling and control of unsteady wake flows. *Phys. Rev.* E **97** (6), 063107.

NAIR, A.G. & TAIRA, K. 2015 Network-theoretic approach to sparsified discrete vortex dynamics. *J. Fluid Mech.* **768**, 549–571.

NEWMAN, M.E.J. 2010 *Networks: An Introduction*. Oxford University Press.

NEWMAN, M.E.J. & GIRVAN, M. 2004 Finding and evaluating community structure in networks. *Phys. Rev.* E **69** (2), 026113.

NEWTON, P.K. 2013 *The N-vortex Problem: Analytical Techniques*. Springer Science & Business Media.

OTTINO, J.M. 1990 Mixing, chaotic advection, and turbulence. *Annu. Rev. Fluid Mech.* **22** (1), 207–254.

REICHARDT, J. & BORNHOLDT, S. 2006 Statistical mechanics of community detection. *Phys. Rev.* E **74** (1), 016110.

RUBINOV, M. & SPORNS, O. 2010 Complex network measures of brain connectivity: uses and interpretations. *Neuroimage* **52** (3), 1059–1069.

SCARSOGLIO, S., CAZZATO, F. & RIDOLFI, L. 2017 From time-series to complex networks: application to the cerebrovascular flow patterns in atrial fibrillation. *Chaos* **27** (9), 093107.

SCHLUETER-KUCK, K.L. & DABIRI, J.O. 2017 Coherent structure colouring: identification of coherent structures from sparse data using graph theory. *J. Fluid Mech.* **811**, 468–486.

SCHMID, P.J. 2010 Dynamic mode decomposition of numerical and experimental data. *J. Fluid Mech.* **656**, 5–28.

SCHNEIDE, C., PANDEY, A., PADBERG-GEHLE, K. & SCHUMACHER, J. 2018 Probing turbulent superstructures in Rayleigh–Bénard convection by Lagrangian trajectory clusters. *Phys. Rev. Fluids* **3** (11), 113501.

SER-GIACOMI, E., ROSSI, V., LÓPEZ, C. & HERNÁNDEZ-GARCÍA, E. 2015 Flow networks: a characterization of geophysical fluid transport. *Chaos* **25** (3), 036404.

SINGH, J., BELUR VISHWANATH, R., CHAUDHURI, S. & SUJITH, R.I. 2017 Network structure of turbulent premixed flames. *Chaos* **27** (4), 043107.

SPENCER, R.S. & WILEY, R.M. 1951 The mixing of very viscous liquids. *J. Colloid Sci.* **6** (2), 133–145.

TAIRA, K., BRUNTON, S.L., DAWSON, S.T.M., ROWLEY, C.W., COLONIUS, T., MCKEON, B.J., SCHMIDT, O.T., GORDEYEV, S., THEOFILIS, V. & UKEILEY, L.S. 2017 Modal analysis of fluid flows: an overview. *AIAA J.* **55** (12), 4013–4041.

TAIRA, K., HEMATI, M.S., BRUNTON, S.L., SUN, Y., DURAISAMY, K., BAGHERI, S., DAWSON, S.T.M. & YEH, C.-A. 2020 Modal analysis of fluid flows: applications and outlook. *AIAA J.* **58** (3), 998–1022.

TAIRA, K., NAIR, A.G. & BRUNTON, S.L. 2016 Network structure of two-dimensional decaying isotropic turbulence. *J. Fluid Mech.* **795**, R2.

YEH, C.-A., GOPALAKRISHNAN MEENA, M. & TAIRA, K. 2021 Network broadcast analysis and control of turbulent flows. *Journal of Fluid Mechanics*, **910**, A15 https://doi:10.1017/jfm.2020.965.

YU, H., KANOV, K., PERLMAN, E., GRAHAM, J., FREDERIX, E., BURNS, R., SZALAY, A., EYINK, G. & MENEVEAU, C. 2012 Studying Lagrangian dynamics of turbulence using on-demand fluid particle tracking in a public turbulence database. *J. Turbul.* **13**, N12.

ZEFF, B.W., LANTERMAN, D.D., MCALLISTER, R., ROY, R., KOSTELICH, E.J. & LATHROP, D.P. 2003 Measuring intense rotation and dissipation in turbulent flows. *Nature* **421** (6919), 146–149.